

## RESEARCH ARTICLE

# Large field of view aberrations correction with deformable lenses and multi conjugate adaptive optics

T. Furieri<sup>1,2</sup> | A. Bassi<sup>3</sup> | S. Bonora<sup>1</sup> 

<sup>1</sup>Institute of Photonics and Nanotechnology, National Council of Research of Italy, Padova, Italy

<sup>2</sup>Department of Information Engineering, University of Padova, Padova, Italy

<sup>3</sup>Department of Physics, Politecnico di Milano, Milan, Italy

## Correspondence

S. Bonora, National Council of Research of Italy, Institute of Photonics and Nanotechnology, via Trasea 7, 35131 Padova, Italy.  
Email: [stefano.bonora@pd.ifi.nr.it](mailto:stefano.bonora@pd.ifi.nr.it)

## Funding information

Horizon 2020 Framework Programme; Laserlab-Europe, Grant/Award Number: 871124; Office of Naval Research Global; Air Force Research Laboratory (AFRL), Grant/Award Number: GRANT12789919; European Union's NextGenerationEU Programme, Grant/Award Numbers: CUP B53C22001750006, ID D2B8D520, IR0000016

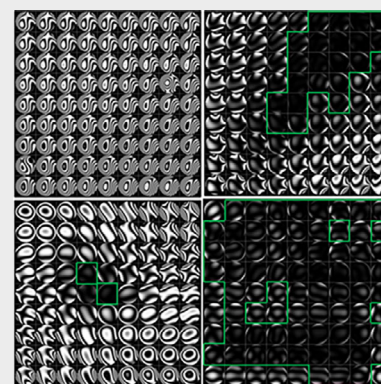
## Abstract

Optical microscopes can have limited resolution due to aberrations caused by samples and sample holders. Using deformable mirrors and wavefront sensorless optimization algorithms can correct these aberrations, but the correction is limited to a small area of the field of view. This study presents an adaptive optics method that uses a series of plug-and-play deformable lenses for large field of view wavefront correction.

A direct wavefront measurement method using the spinning sub-pupil aberration measurement technique is combined with correction based on the deformable lenses. Experimental results using fluorescence microscopy with a wide field and a light sheet fluorescence microscope show that the proposed method can achieve detection and correction over an extended field of view with a compact transmissive module placed in the detection path of the microscope. This method could improve the resolution and accuracy of imaging in a variety of fields, including biology and materials science.

## KEYWORDS

adaptive optics, deformable lenses, light sheet microscope, wavefront correction



## 1 | INTRODUCTION

Adaptive optics (AO) is a technology used to enhance image quality when an optical system is affected by phase aberrations. In optical microscopy, these aberrations can occur due to imperfections or misalignment of the illumination or detection optics. This is especially relevant with the continuous development of new microscopy configurations and measurement protocols, such as clearing

methods [1, 2] or customized sample holders [3, 4]. On the other hand, inhomogeneities in the refractive index of the sample can cause aberrations or decrease the contrast of the acquired images. To achieve high-resolution and super-resolution imaging, a thorough understanding of these aberrations, along with their correction, is necessary.

Recently, various approaches have been developed to compensate for optical aberrations in microscopy [5, 6]

This is an open access article under the terms of the [Creative Commons Attribution-NonCommercial-NoDerivs](https://creativecommons.org/licenses/by-nc-nd/4.0/) License, which permits use and distribution in any medium, provided the original work is properly cited, the use is non-commercial and no modifications or adaptations are made.

© 2023 The Authors. *Journal of Biophotonics* published by Wiley-VCH GmbH.

such as using a deformable mirror or a liquid crystal spatial light modulator placed in the pupil or image plane of the optical system. However, AO with a closed loop control (which is an approach typically used in astronomy), is not practical in microscopy, because samples may not have bright point sources for wavefront sensing. As a result, wavefront sensorless control has become a standard for AO in microscopy with main advancements achieved through image sharpening [6, 7] and pupil segmentation techniques [8, 9]. Image sharpening uses a merit function which displays a maximum when the aberrations are minimized. With this assumption it is easy to apply some bias aberrations to estimate the wavefront error using an optimization algorithm and then compensate for them. Pupil segmentation is based on a different method: by means of a liquid crystal panel, the pupil is segmented and the tilt in each segment is tuned as the signal is being optimized.

Although AO has demonstrated its benefits, several limitations are still hindering its widespread diffusion. In fact, the level of the correction depends on the sample structure, and it is not measurable, together with the correction being limited to the isoplanatic patch, which is often smaller than the field of view. In addition, microscopes must be entirely redesigned to include AO, adding complexity and limiting its adoption in commercial systems.

Some of these problems have been recently approached, but a method that solves them together is not yet available. For example [10–12], proposed methods that strongly simplify the system using an adaptive lens, instead of a deformable mirror, combined with optimization algorithms. This has brought to promising results in microscopy and ophthalmic imaging [7, 13]. The limited isoplanatic correction has been addressed with different techniques, such as multi-conjugate AO, using two deformable mirrors [14, 15], or anisoplanatic correction with liquid crystals [16]. The dependence on the sample structure and contrast has been analyzed and solved adding high spatial frequencies in the illumination path [17]. References [18, 19] present a solution based on a combination of hardware and software correction using deconvolution.

In this paper we present a solution for extending isoplanatic correction, direct wavefront measurement and correction, in a transmissive setup. We introduce a simple and compact optical module, able to measure and correct the aberrations over an extended field of view, using a standard microscope objective lens.

To detect the aberrations, we use the spinning pupil aberration measurement (SPAM) described in [18]. The SPAM scans the microscope optical pupil with a small sub aperture, reconstructing the phase aberration on the entire field of view. We integrate this measurement with aberration correction in a single, compact device. The

correction is achieved using adaptive lenses, based on multiple piezoelectric actuators, that fit into the same chassis of the SPAM module. We demonstrate that using a combination of two different adaptive lenses, placed on and outside the pupil plane, we can achieve anisoplanatic wavefront correction on a large field of view, in a conventional and light sheet microscope.

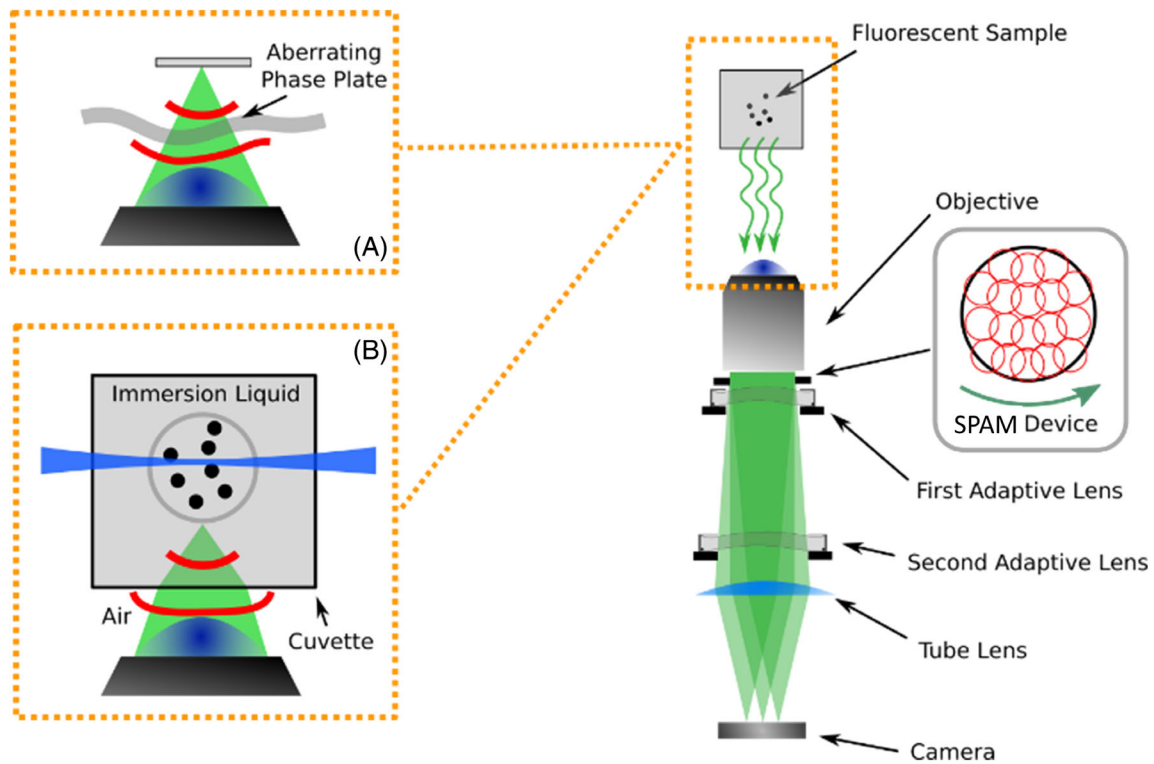
## 2 | MATERIALS AND METHODS

### 2.1 | Adaptive optics

In our experiments, we used a multi actuator adaptive lens, which is similar to the one described in reference [10]. The lens employs ultrathin glass membranes that are curved by piezoelectric actuators. The space in between two glass membranes is filled with transparent liquid, and each face is mounted with a piezoelectric actuator ring segmented into nine parts for a total of 18 individually controllable actuators. This allows the lens to produce aberrations up to the fourth order Zernike polynomials. The optical properties of the lens we used in the study are provided in the Supplementary Text in Tables S4 and S5.

### 2.2 | Wavefront measurement and closed loop control

The wavefront measurement system is the same used in reference [18]. It comprises a rotating wheel that scans the pupil with an iris of 2.5 mm. The scan is performed at 4 radial distances, with the iris angular positions designed to sample all the pupil, as shown in Figure 1. This system samples the wavefront at 18 points, requiring 18 images to be acquired for each measurement. Our tests confirm that this sampling scheme is adequate for precise measurements of wavefronts up to the fourth order of Zernike polynomials. The exposure time is automatically adjusted based on the ratio  $R$  of the sub-aperture area to the pupil area, and the total measurement time is about 12 s. We used the wavefront measurement to characterize the deformable lenses required for closed-loop control, storing the wavefront deformation of each actuator in an influence functions matrix. Before the experiment, we performed this characterization by poking each actuator individually while using a phantom target positioned at 9 equally spaced points in a  $3 \times 3$  grid across the field of view. During the correction process, we could choose the positions used for wavefront correction, as shown in Figure 3. Further information on the closed-loop control is available in the [supplementary material](#).



**FIGURE 1** Optical layout of the imaging system used in this experiment including the SPAM module and the two adaptive lenses. The microscope has been used in wide field and light sheet microscopy configuration, as shown in insets (A) and (B). SPAM, spinning pupil aberration measurement.

### 2.3 | Light-sheet fluorescence microscope

We used a customized light sheet fluorescence microscopy system that is similar to the one described in reference [20]. The system comprised a diode-pumped solid-state laser that emitted light at 473 nm, which was coupled through a single-mode optical fiber to the sample. The laser beam was collimated to a 2 mm waist and passed through a cylindrical lens with a focal length of 50 mm, and the illumination power was set at 1.2 mW. The fluorescence signal was collected using a long working distance objective (Mitutoyo, NA = 0.28, WD = 34 mm) with a 10 $\times$  magnification. The objective, together with a tube lens and a long pass filter (FELH500, Thorlabs), formed the image on a CMOS camera (ORCA Flash 4.0, Hamamatsu) with a field of view of approximately 11  $\times$  11 mm. The sample was placed in a 20  $\times$  20 mm glass cuvette and was moved with a 3-axis stage.

### 2.4 | Zebrafish brain

For imaging the zebrafish brain we reused a sample prepared previously. The details of sample preparation, that

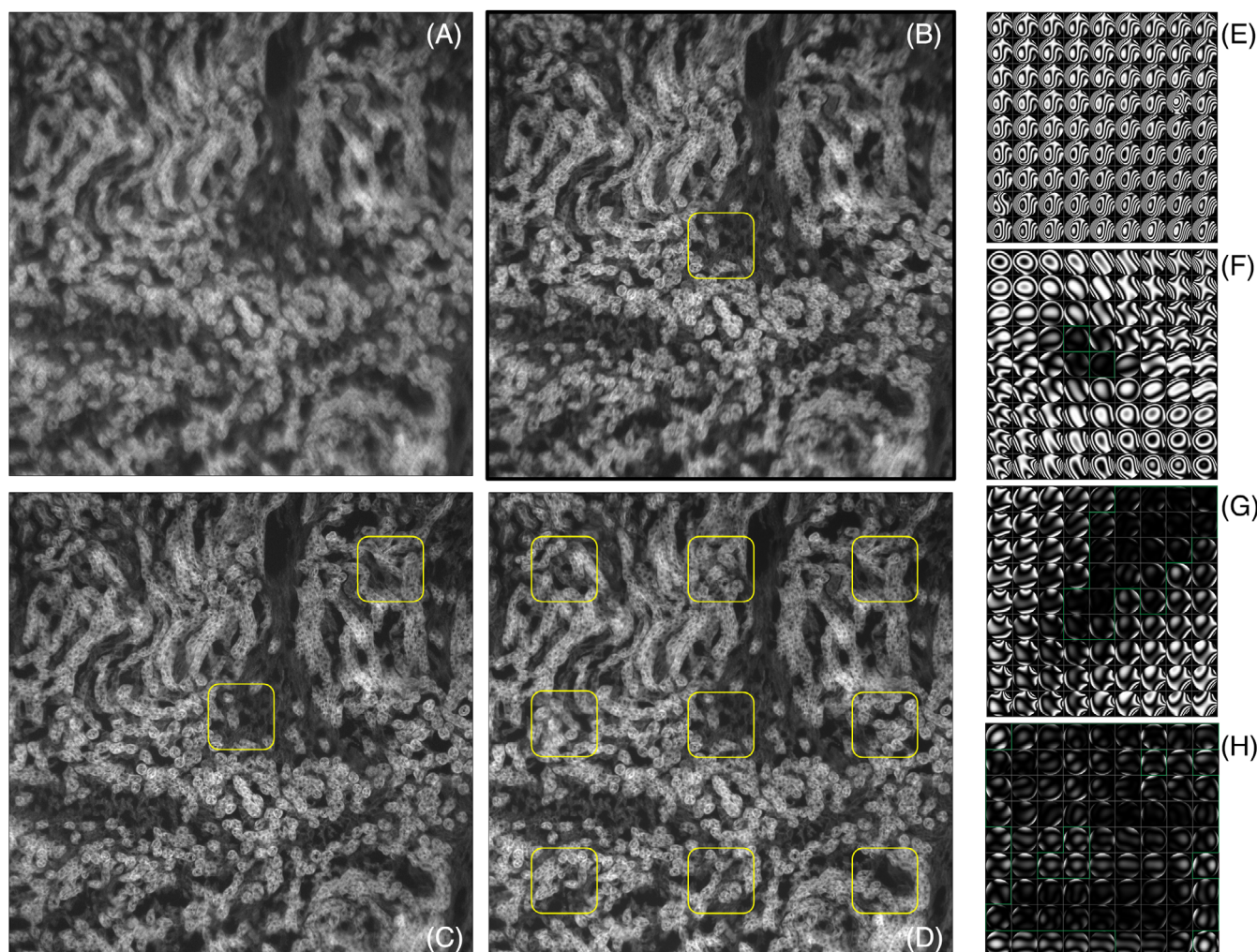
was in accordance with the protocol n. 513/2018-PR, authorized on July 4, 2018 by the Italian Health Ministry, are described in [19]. The autofluorescence visible in Figure 3 is mainly derived from blood-containing brain vessels.

## 3 | RESULTS AND DISCUSSION

### 3.1 | Integrated wavefront aberration measurement and correction

The developed device incorporates both wavefront measurement and correction. The latter is obtained using adaptive lenses made of ultrathin glass membranes bended by multiple piezoelectric actuators [10]. These lenses are compact and can be placed directly in the detection path of the optical microscope. Adjacent to the lens, we placed a spinning sub-aperture module, able to measure the wavefront aberrations. The founding idea of this device is to sample the wavefront by moving the sub-aperture inside the pupil and to measure the relative shift of each acquired image. Details of this wavefront measurement techniques can be found in [18].

By measuring the wavefront, we were able to implement the same type of closed loop control system used in conventional AO systems [21]. The control system



**FIGURE 2** Each panel shows an image of the sample and the interferograms of the measured aberrations in a  $9 \times 9$  measurement regions each of them consisting in  $210 \times 210$  pixels. (A) Aberrated image without AL, (B) Image correction with two ALs in the central field, (C) Aberration correction with two ALs central and lateral field, (D) Aberration correction with two ALs in six positions. The corrected fields are highlighted in red. Scale bar is  $200\mu\text{m}$  (see Visualization 1–4 for the full resolution images). The yellow squares (A–D) and square (E–H) mark the corrected position by the closed loop system. The green lines show the portion of the image below the Marechal criterion.

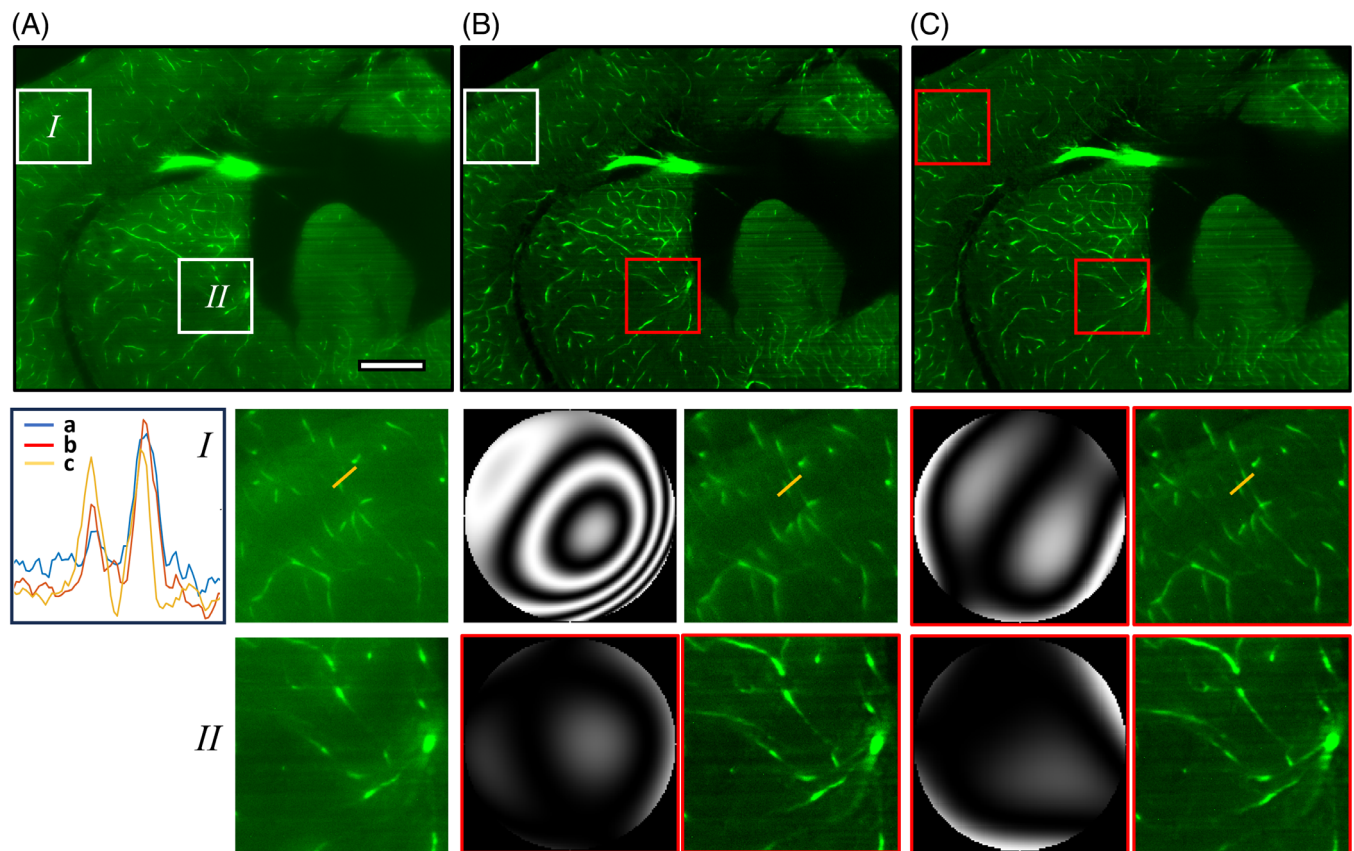
computes the actuators control voltages that minimize the wavefront deviation from flat using an integrative controller. Differently to wavefront sensorless algorithms, the presented SPAM system does not depend on the sample structure, representing a strong advantage particularly in optical microscopy.

### 3.2 | Aberrations correction on an extended area

Adaptive optics has a key drawback in that it only corrects a small, defined area around the correction point. The size of this region, known as the isoplanatic patch, varies based on the presence of volumetric aberrations [16, 21, 22]. To address this limitation in astronomy, a

technique known as multi conjugate adaptive optics (MCAO) has been developed [23, 24]. With MCAO, multiple deformable mirrors are used to correct the wavefront, resulting in a larger isoplanatic patch and a more extensive corrected field of view. The size of the corrected field ultimately depends on the distribution of the aberrations in the volume of the object space and the capability of the wavefront modulators to compensate for them in the image space. However, it is worth noting that while aberrations occur throughout the entire volume, correction takes place in two planes (based on the number of modulators used), with the goal of maximizing the corrected field size and, as a consequence a full field of view correction may not always be achievable.

The implementation of MCAO in microscopy has been challenging, due to the difficulties in incorporating



**FIGURE 3** Light sheet microscopy acquisition of a chemically cleared adult zebrafish brain section, without and with correction. The fluorescent signal arises from blood-containing brain vessels. (A) Without the adaptive lenses (removed from the detection system). (B) Correction only in the center of the field of view (red region). (C) Correction in the center of the field of view and at the top left. Two insets (I, II) are shown for each acquisition, with the corresponding wavefront phases. The corrected regions are shown in red. Scale bar is 200  $\mu\text{m}$ . The inset shows the cross sections obtained from Figures A–C. The cross-section size is 115  $\mu\text{m}$ . The cross-section position is highlighted in the figures with a yellow line.

multiple deformable mirrors in the detection path of a microscope, and the lack of a wavefront measurement system. Our approach addresses these challenges by incorporating two critical components: the SPAM method is used for the wavefront measurement system and a series of multi-actuator deformable lenses are employed for wavefront correction. Our wavefront reconstruction algorithm, which is equivalent to the Shack–Hartmann method, along with our MCAO control, are further explained in Section 2. The schematic of the system is shown in Figure 1A, the SPAM module (18 actuators Adaptive Lens with 10 mm pupil, AOL1810 Dynamic Optics srl) and spinning pupil is placed in proximity of the back aperture of the objective lens (long working distance Mitutoyo NA = 0.28 10 $\times$ ). At 92 mm from the back-aperture we placed the second AL with 18 actuators and a 16 mm clear aperture (AOL1816, Dynamic Optics srl). The position of this lens was chosen to completely illuminate its clear aperture. Avoiding to underfill its aperture, and therefore decreasing its capacity of wavefront modulation, or overfill it creating vignetting.

The calibration process in our technique is comparable to the one used in a standard AO setup. The main difference is that we simultaneously consider the wavefront measurement in multiple points of the field of view. The controller, in this case, minimizes the wavefront error for all the selected fields. More details on the controller can be found in reference [25]. In order to demonstrate that the proposed method allows for the extension of the corrected area in optical microscopy, we initially tested it on a wide field fluorescence microscope at 10 $\times$  magnification, with NA = 0.28. We imaged a test slide (Fluocell sample prepared slice #3), with a mouse kidney section labeled with Alexa Fluor™ 488 WGA, having a phase plate placed in front of it, to induce controlled aberrations (Figure 1A). In the first experiment, the lenses were in their flat position. We measured the wavefront after the introduction of the phase plate in 9  $\times$  9 positions of the image as shown in Figure 1A. The measurements (summarized in Table 1) indicate that the image resolution decreases due to the variation of the wavefront aberrations, which vary field to field with

**TABLE 1** Comparison of the correction parameter for the wide field fluorescence microscope. The table reports the area (%) of the image below the Marechal criterion, the residual wavefront error in the corrected image segment (highlighted in red in Figure 2) and the average wavefront error on the whole image.

	Below lambda/14 @530 nm (%)	Segment rms error (waves@530 nm)	Mean image rms error (waves@530 nm)
<b>Without AL</b>	0		0.78
<b>Two AOLs one position corrected</b>	3.7	0.04—center	0.33
<b>Two AOLs two positions corrected</b>	28.4	0.03—center 0.03—top right	0.15
<b>Two AOLs six positions corrected</b>	90	Top row: 0.03 0.05 0.07 Central row: 0.07 0.06 0.06 Bottom row: 0.04 0.03 0.04	0.06

an average value of 0.78 waves rms (@530 nm). As a second step, we corrected the wavefront in a single point of the image. We repeated such measurement correcting both the center and the top-right corner using AOL<sub>1</sub> and AOL<sub>2</sub> (see Figure 2B,C). The results show that the adaptive lenses can effectively correct nearly all the aberrations. Although only a small portion in the nearby of the corrected area respects the Marechal criterion for a well corrected system (rms error of the aberration <0.08 waves rms, see the green contours in the respective interferograms E–G), the whole image benefits from the wavefront correction in both experiments. The average aberration error on the whole image was of 0.33 waves rms (central point), 0.15 waves rms (center and top right point) while the portion of image being well corrected is 3.7% and 28%, respectively (Figure 2C). In the measurement reported in Figure 2D we applied simultaneously the correction in six points (yellow squares). This results in a complete correction on 90% of the image with an average rms wavefront error of 0.06 waves rms. A summary of these data is reported in Table 1.

### 3.3 | Aberrations measurement and correction in a light-sheet fluorescence microscope

The proposed device for measuring and correcting aberrations in a wide field configuration is a valuable addition to the field of light sheet fluorescence microscopy (LSFM) [26]. This cutting-edge microscopy technique illuminates a single plane of a three-dimensional fluorescent sample and uses widefield detection optics to collect light orthogonally to the excitation plane. This selective illumination provides intrinsic optical sectioning capability, making it a powerful tool for three-dimensional imaging of biological samples. This is especially useful for large, chemically cleared specimens, such as entire organisms, small animal organs and

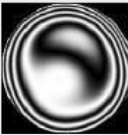

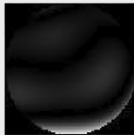
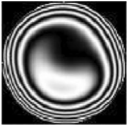
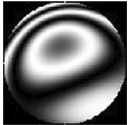

tissues. When using LSFM to image these types of specimens, they are typically placed in a high refractive index medium, like gels or solvents, and placed in a glass cuvette to avoid the contact between the solvent and the objective-lenses. However, using a high refractive index medium and a glass cuvette can result in aberrations that can distort the image. In LSFM, cleared specimens that are typically a few millimeters to centimeters in size are placed in a high refractive index medium with a refractive index of approximately  $n \approx 1.4$  for samples cleared in gel-based media such as clarity [2], and  $n \approx 1.5$  for samples cleared in solvents like benzyl benzoate and dibenzyl-ether [23].

To avoid these aberrations, a specialized long working distance microscope objective lens is often required. To demonstrate that the proposed technique for measuring and correcting aberrations is compatible with the use of standard long working distance microscope objective lenses, we used a LSFM microscope based on cylindrical lens illumination. They placed the aberration correction module in the detection arm of the microscope, directly after the objective lens. This placement allows for real-time correction of any aberrations that may occur, resulting in improved image quality and accuracy.

To prove that the technique for measuring and correcting aberrations can be used with standard long working distance microscope objective lenses, we applied the method to a LSFM microscope based on cylindrical lens illumination. The aberration correction module was placed in the detection arm of the microscope, immediately after the objective lens, allowing for real-time correction of potential aberrations for improved image quality.

It is worth noting that the proposed method to correct aberrations could also be used in LSFM illumination. Nonetheless, the light sheet thickness was relatively large (the beam waist was c.a. 7  $\mu\text{m}$ ) so to have a uniform light sheet thickness over the entire field of view, with negligible illumination aberrations.

TABLE 2 Wavefront data relative to the fluorescent beads acquisition.

	No AOL FWHM ( $\mu\text{m}$ )	AOL Corrected FWHM ( $\mu\text{m}$ )	No AOL Rms error (waves)	AOL—center corrected Rms error (waves)	AOL—center + corner corrected Rms error (waves)
Theoretical	1.1				
Center	1.79	1.35	0.54	0.01	0.04
					
Corner	2.3	1.57	0.69	0.23	0.05
					

Initially, we conducted a test on commercially available fluorescence beads (Estapor F1-XC 010). These polystyrene microspheres have a diameter of 160 nm on average, which is significantly below the diffraction limit, and exhibit two fluorescence peaks at 525 and 560 nm. A solution of 1:4000 beads in water was embedded in 1.5% phytigel and placed in a fluorinated ethylene propylene tube with a refractive index similar to water. The tube was then inserted into an optical glass cuvette, with rectangular base, filled with distilled water for imaging purposes. Our results revealed the presence of a significant spherical aberration caused by the interface between air and water in the cuvette, especially in off-axis fields, where it produced a coma component. Table 2 provides a summary of the measurements. Correction applied only at the central point, previously reported, led to a small residual error (0.01waves) but still left a significant coma component in the off-axis point (0.23waves rms). The bead FWHM was improved from 1.79 to 1.35  $\mu\text{m}$ , indicating an improvement in resolution. Correction applied at both the central and corner points, using two AOLs, reduced the residual error to 0.04waves and 0.05waves rms, respectively. The bead profile in the corner of the image was reduced to 1.57  $\mu\text{m}$ .

Next, we imaged an unstained but autofluorescent zebrafish brain, primarily fluorescent in the blood vessels. Figure 3 displays the results, with two sample regions where wavefront correction was applied. These regions correspond to the optic tectum (fields I) and the diencephalon (II). We first removed any adaptive lens from the microscope for a fair comparison and acquired the image, as seen in Figure 3A. After inserting the adaptive lenses for wavefront correction, we observed a clear improvement in contrast in the central field (Figure 3B). The wavefront measurements (Table 3) indicate that the aberration was almost entirely corrected in field II

TABLE 3 Wavefront error data relative to the aberration correction of the Zebrafish brain of Figure 3.

RMS (waves @530 nm)	Zone I correction	Zone I and zone II correction
Zone I	0.32	0.10
Zone II	0.05	0.06
Mean RMS in the two zones	0.19	0.08

(0.05waves RMS) while residual coma remained in the corner (field I, 0.32waves RMS). However, the overall image quality was still higher than the initial image.

Figure 3C shows the images once the wavefront correction is applied on two fields (I and II, see results in Table 3). These results suggest that aberrations can be effectively measured and corrected over the entire field of view using two adaptive lenses. The correction led to an enlargement of the isoplanatic patch and an increase in contrast across the entire image.

## 4 | CONCLUSIONS

In this study, we investigated the use of a stack of deformable lenses for increasing the correction area in fluorescence microscopy. Our results show that the use of deformable lenses is a simple and implementable solution for AO compared to deformable mirrors or liquid crystal spatial light modulators. We integrated the adaptive-lenses-based correction with a recently developed aberration-detection method, named SPAM, which allows for direct measurement of wavefronts from the detected image. This method provides quantitative information about the phase aberration generated by the

sample, making it an important tool for evaluating the optical performance of a microscope assessing the size of the well-corrected patch after wavefront correction. With respect to the widely used wavefront sensorless approach this method present the advantage of the possibility to measure from the wavefront data both the level of the correction and the size of the corrected field of view without adding complexity to the system being the measurement device integrated inside the deformable lens.

We found that even though the part of the image with diffraction-limited features is small (around 4%), the overall image benefits from correction, as evidenced by a decrease in RMS wavefront error from 0.78 waves to about 0.3 waves. This further supports the use of two wavefront modulators.

In conclusion, our results demonstrate the effectiveness of using two deformable lenses in correcting aberrations in optical microscopy. The SPAM detection provides a convenient and robust method for evaluating the optical performance of microscopes, while the correction results justify the use of two wavefront modulators. The integration of deformable lenses with the SPAM detection system into a single device offers a simple solution for installing aberration correction on any type of widefield microscope.

## ACKNOWLEDGMENTS

CNR-IFN was supported by Office of Naval Research global (ONRG) and by Air Force Research Laboratory (AFRL) with grant GRANT12789919. Politecnico of Milan has received funding from LASERLAB-EUROPE (grant agreement no. 871124, European Union's Horizon 2020 research and innovation programme) and the European Union's NextGenerationEU Programme with the I-PHOQS Infrastructure (IR0000016, ID D2B8D520, CUP B53C22001750006) "Integrated infrastructure initiative in Photonic and Quantum Sciences."

## CONFLICT OF INTEREST STATEMENT

The authors declare no conflict of interest.

## DATA AVAILABILITY STATEMENT

The data that support the findings of this study are available from the corresponding author upon reasonable request.

## ORCID

S. Bonora  <https://orcid.org/0000-0002-5049-7049>

## REFERENCES

- [1] A. Ertürk, F. Bradke, *Exp. Neurol.* **2013**, *242*, 57.
- [2] K. Chung, J. Wallace, S. Y. Kim, S. Kalyanasundaram, A. S. Andalman, T. J. Davidson, J. J. Mirzabekov, K. A. Zalocusky,

- J. Mattis, A. K. Denisin, S. Pak, H. Bernstein, C. Ramakrishnan, L. Grosenick, V. Gradinaru, K. Deisseroth, *Nature* **2013**, *497*, 332.
- [3] A. Kaufmann, M. Mickoleit, M. Weber, J. Huisken, *Development* **2012**, *139*, 3242.
- [4] R. Tomer, M. Lovett-Barron, I. Kauvar, A. Andalman, V. M. Burns, S. Sankaran, L. Grosenick, M. Broxton, S. Yang, K. Deisseroth, *Cell* **2015**, *163*, 1796.
- [5] N. Ji, *Nat. Methods* **2017**, *14*, 374.
- [6] M. J. Booth, *Light. Appl.* **2014**, *3*, e165.
- [7] H. R. G. W. Verstraete, M. Heisler, M. J. Ju, D. Wahl, L. Bliet, J. Kalkman, S. Bonora, Y. Jian, M. Verhaegen, M. V. Sarunic, *Biomed. Opt. Express* **2017**, *8*, 2261.
- [8] N. Ji, D. E. Milkie, E. Betzig, *Nat. Methods* **2010**, *7*, 141.
- [9] D. J. Wahl, C. Huang, S. Bonora, Y. Jian, M. V. Sarunic, *Opt. Lett.* **2017**, *42*, 1365.
- [10] S. Bonora, Y. Jian, P. Zhang, A. Zam, E. N. Pugh, R. J. Zawadzki, M. V. Sarunic, *Opt. Express* **2015**, *23*, 21931.
- [11] P. Pozzi, M. Quintavalla, A. B. Wong, J. G. G. Borst, S. Bonora, M. Verhaegen, *Opt. Lett.* **2020**, *45*, 3585.
- [12] K. Banerjee, P. Rajaeipour, Ç. Ataman, H. Zappe, *Appl. Opt.* **2018**, *57*, 6338.
- [13] M. Skorsetz, P. Artal, J. M. Bueno, *J. Microsc.* **2016**, *261*, 249.
- [14] M. Laslandes, M. Salas, C. K. Hitzengerger, M. Pircher, *Biomed. Opt. Express* **2017**, *8*, 4811.
- [15] J. Thaug, P. Knutsson, Z. Popovich, M. Owner-Petersen, *Opt. Express* **2009**, *17*, 4454.
- [16] P. Pozzi, C. Smith, E. Carroll, D. Wilding, O. Soloviev, M. Booth, G. Vdovin, M. Verhaegen, *Opt. Express* **2020**, *28*, 14222.
- [17] M. Žurauskas, I. M. Dobbie, R. M. Parton, M. A. Phillips, A. Göhler, I. Davis, M. J. Booth, *Optica* **2019**, *6*, 370.
- [18] D. Ancora, T. Furieri, S. Bonora, A. Bassi, *Opt. Lett.* **2021**, *46*, 2884.
- [19] T. Furieri, D. Ancora, G. Calisesi, S. Morara, A. Bassi, S. Bonora, *Biomed. Opt. Express* **2022**, *13*, 262.
- [20] L. Maiuri, A. Candeo, I. Sana, E. Ferrari, C. D'Andrea, G. Valentini, A. Bassi, *J. Biomed. Opt.* **2016**, *21*, 56001.
- [21] J. Li, D. R. Beaulieu, H. Paudel, R. Barankov, T. G. Bifano, J. Mertz, *Optica* **2015**, *2*, 682.
- [22] J. Mertz, H. Paudel, T. G. Bifano, *Appl. Opt.* **2015**, *54*, 3498.
- [23] R. Ragazzoni, E. Marchetti, G. Valente, *Nature* **2000**, *403*, 54.
- [24] J. Thaug, P. Knutsson, Z. Popovic, M. Owner-Petersen, *Opt. Express* **2009**, *17*, 4454.
- [25] R. K. Tyson, *Introduction to Adaptive Optics*. **2009**.
- [26] O. E. Olarte, J. Andilla, E. J. Gualda, P. Loza-Alvarez, *Adv. Opt. Photon.* **2018**, *10*, 111.

## SUPPORTING INFORMATION

Additional supporting information can be found online in the Supporting Information section at the end of this article.

**How to cite this article:** T. Furieri, A. Bassi, S. Bonora, *J. Biophotonics* **2023**, *16*(12), e202300104. <https://doi.org/10.1002/jbio.202300104>